Supplementary information for "Spin-phonon interactions and magnetoelectric coupling in $Co_4B_2O_9$ (B = Nb, Ta)"

K. Park *et. al.*

(Dated: February 22, 2023)

CONTENTS

I. VIBRATIONAL MODE SYMMETRIES IN $CO_4NB_2O_9$ AND THE TA ANALOG

Group theory reveals that a material with space group $P\bar{3}c1$ also has a point group of D_{3d}. Table S1 shows the symmetry elements and irreducible representations of D_{3d}. Several things are immediately apparent. Modes of A_{2u} and E_u symmetry are infrared-active, whereas modes of A_{1g} and E_g symmetry are Raman-active. These features transform as "change in dipole" and "change in polarizability", respectively. Focusing on the infrared-active modes, E_u is doubly-degenerate and contains both the x and y matrix elements. We observe these features in the ab-plane measurement of $Co_4Nb_2O_9$ and the Ta analog. On the other hand, the singly-degenerate A_{2u} symmetry modes appear in the c-axis polarization because they transform as "z" in the character table below.

$\mathbf{D}_{3d}$	E	$2C_3$	$3C_2'$	i	$2S_6$	$3\sigma_d$	Matrix element
A_{1g}	+1	+1	+1	+1	+1	+1	(x^2+y^2, z^2)
A_{2g}	+1	+1	-1	+1	+1	-1	-
E_g	+2	-1	0	+2	-1	0	$(x^2-y^2, xz)(yz, xy)$
A_{1u}	+1	+1	+1	-1	-1	-1	-
A_{2u}	+1	+1	-1	-1	-1	+1	z
E_u	+2	-1	0	-2	+1	0	(x, y)

TABLE S1. Character table for the D_{3d} point group. Based upon symmetry, we expect to see doubly-degenerate E_u vibrational modes in the ab-plane infrared response whereas we anticipate A_{2u} symmetry modes to be polarized along the c-axis.

We also predict the number of phonon modes by using the symmetry analysis tool.[S1] Table S2 summarizes each allowed Wyckoff position for infrared-active modes. As predicted by the character table, A_{2u} and E_u modes are infrared-active, A_{1g} and E_g modes are Raman-active. For infrared, there are a total of 8 for A_{2u} mode and 15 for E_u mode with acoustic modes (A_{2u} + E_u). By subtracting acoustic modes, we, therefore, have 7 of A_{2u} modes and 14 of E_u modes. For Raman, there are 7 of A_{1g} and 15 of E_g modes.

Atoms	WP	A_{1g}	A_{1u}	A_{2g}	A_{2u}	E_u	E_g
Nb	4c	1	·	·	1	2	2
Co1	4d	1	·	·	1	2	2
Co2	4d	1	·	·	1	2	2
O1	6f	1	·	·	2	3	3
O2	12g	3	·	·	3	6	6

TABLE S2. Selection rules for infrared- and Raman-active modes on each Wyckoff position.[S1] *WP = Wyckoff position

We used another tool to calculate displacements for A_{2u} and E_u modes in order to distinguish each atom's contribution to A_{2u} and E_u modes. We only included these two since we are only interested in the infrared-active modes.[S2] Table S3 displays each atom's position in Cartesian coordinates with respect to the unit cell. The total number of atoms is 30 with 4 Nb, 4 Co1, 4 Co2, 6 O1, and 12 O2 atoms in the unit cell. Now, Tables. S4 and S5 are showing the dynamical matrix for each mode in the unit cell, which shows displacement patterns for each mode.

TABLE S3: Atomic positions in the unit cell.[S2]

atom	type	x	y	z
1	Nb	0.00000	0.00000	2.01081
2	Nb	0.00000	0.00000	5.06204
3	Nb	0.00000	0.00000	12.13489
4	Nb	0.00000	0.00000	9.08366
5	Co1	0.00000	2.98698	2.73069
6	Co1	2.58680	1.49349	4.34216
7	Co1	2.58680	1.49349	11.41501
8	Co1	0.00000	2.98698	9.80354
9	Co2	0.00000	2.98698	13.95091
10	Co2	2.58680	1.49349	7.26764
11	Co2	2.58680	1.49349	0.19479
12	Co2	0.00000	2.98698	6.87806
13	O1	0.00000	0.00000	3.53642
14	O1	0.00000	0.00000	3.53642
15	O1	0.00000	0.00000	3.53642

16	O1	0.00000	0.00000	10.60928
17	O1	0.00000	0.00000	10.60928
18	O1	0.00000	0.00000	10.60928
19	O2	-1.64288	3.05613	1.19814
20	O2	0.76155	1.52963	1.19814
21	O2	0.88132	4.37518	1.19814
22	O2	0.94392	1.42434	5.87471
23	O2	3.46812	0.10529	5.87471
24	O2	3.34835	2.95084	5.87471
25	O2	4.22968	1.42434	12.94756
26	O2	1.82525	2.95084	12.94756
27	O2	1.70548	0.10529	12.94756
28	O2	1.64288	3.05613	8.27099
29	O2	-0.88132	4.37518	8.27099
30	O2	-0.76155	1.52963	8.27099

TABLE S4: Dynamical matrix for the A_{2u} mode.[S2]

Symmetry modes:	A_{2u}	Displacement		
atom	type	x	y	z
1	Nb	0.00000	0.00000	1.00000
2	Nb	0.00000	0.00000	1.00000
3	Nb	0.00000	0.00000	1.00000
4	Nb	0.00000	0.00000	1.00000
5	Co1	0.00000	0.00000	1.00000
6	Co1	0.00000	0.00000	1.00000
7	Co1	0.00000	0.00000	1.00000
8	Co1	0.00000	0.00000	1.00000
9	Co2	0.00000	0.00000	1.00000
10	Co2	0.00000	0.00000	1.00000
11	Co2	0.00000	0.00000	1.00000
12	Co2	0.00000	0.00000	1.00000
13	O1	-0.00000	-1.00000	-0.00000
14	O1	0.86603	0.50000	-0.00000
15	O1	-0.86603	0.50000	-0.00000
16	O1	-0.00000	-1.00000	-0.00000
17	O1	0.86603	0.50000	-0.00000
18	O1	-0.86603	0.50000	-0.00000
13	O1	0.00000	0.00000	1.00000
14	O1	0.00000	0.00000	1.00000
15	O1	0.00000	0.00000	1.00000
16	O1	0.00000	0.00000	1.00000
17	O1	0.00000	0.00000	1.00000
18	O1	0.00000	0.00000	1.00000
19	O2	0.86603	0.50000	0.00000
20	O2	-0.86603	0.50000	0.00000
21	O2	-0.00000	-1.00000	0.00000
22	O2	-0.86603	0.50000	0.00000
23	O2	-0.00000	-1.00000	0.00000
24	O2	0.86603	0.50000	0.00000
25	O2	0.86603	0.50000	0.00000
26	O2	-0.86603	0.50000	0.00000
27	O2	-0.00000	-1.00000	0.00000
28	O2	-0.86603	0.50000	0.00000
29	O2	-0.00000	-1.00000	0.00000
30	O2	0.86603	0.50000	0.00000
19	O2	1.00000	0.00000	0.00000
20	O2	-0.50000	0.86603	0.00000
21	O2	-0.50000	-0.86603	0.00000
22	O2	-1.00000	0.00000	0.00000

23	O2	0.50000	-0.86603	0.00000
24	O2	0.50000	0.86603	0.00000
25	O2	1.00000	0.00000	0.00000
26	O2	-0.50000	0.86603	0.00000
27	O2	-0.50000	-0.86603	0.00000
28	O2	-1.00000	0.00000	0.00000
29	O2	0.50000	-0.86603	0.00000
30	O2	0.50000	0.86603	0.00000
19	O2	0.00000	0.00000	1.00000
20	O2	0.00000	0.00000	1.00000
21	O2	0.00000	0.00000	1.00000
22	O2	0.00000	0.00000	1.00000
23	O2	0.00000	0.00000	1.00000
24	O2	0.00000	0.00000	1.00000
25	O2	0.00000	0.00000	1.00000
26	O2	0.00000	0.00000	1.00000
27	O2	0.00000	0.00000	1.00000
28	O2	0.00000	0.00000	1.00000
29	O2	0.00000	0.00000	1.00000
30	O2	0.00000	0.00000	1.00000

TABLE S5: Dynamical matrix for the E_u mode.[S2]

Symmetry modes:	E_u	Displacement		
atom	type	x	y	z
1	Nb	0.00000	1.00000	0.00000
2	Nb	-0.00000	-1.00000	0.00000
3	Nb	0.00000	1.00000	0.00000
4	Nb	-0.00000	-1.00000	0.00000
1	Nb	1.00000	0.00000	0.00000
2	Nb	1.00000	0.00000	0.00000
3	Nb	1.00000	0.00000	0.00000
4	Nb	1.00000	0.00000	0.00000
5	Co1	0.00000	1.00000	0.00000
6	Co1	-0.00000	-1.00000	0.00000
7	Co1	0.00000	1.00000	0.00000
8	Co1	-0.00000	-1.00000	0.00000
5	Co1	1.00000	0.00000	0.00000
6	Co1	1.00000	0.00000	0.00000
7	Co1	1.00000	0.00000	0.00000
8	Co1	1.00000	0.00000	0.00000
9	Co2	0.00000	1.00000	0.00000
10	Co2	-0.00000	-1.00000	0.00000
11	Co2	0.00000	1.00000	0.00000
12	Co2	-0.00000	-1.00000	0.00000
9	Co2	1.00000	0.00000	0.00000
10	Co2	1.00000	0.00000	0.00000
11	Co2	1.00000	0.00000	0.00000
12	Co2	1.00000	0.00000	0.00000
13	O1	1.00000	0.00000	0.00000
14	O1	0.25000	-0.43301	0.00000
15	O1	0.25000	0.43301	0.00000
16	O1	1.00000	0.00000	0.00000
17	O1	0.25000	-0.43301	0.00000
18	O1	0.25000	0.43301	0.00000
14	O1	1.00000	0.57735	-0.00000
15	O1	1.00000	-0.57735	-0.00000
17	O1	1.00000	0.57735	-0.00000
18	O1	1.00000	-0.57735	-0.00000
14	O1	0.00000	0.00000	1.00000

15	O1	-0.00000	-0.00000	-1.00000
17	O1	0.00000	0.00000	1.00000
18	O1	-0.00000	-0.00000	-1.00000
20	O2	0.86603	-0.50000	-0.00000
21	O2	-0.00000	-1.00000	-0.00000
23	O2	0.00000	1.00000	-0.00000
24	O2	0.86603	0.50000	-0.00000
26	O2	0.86603	-0.50000	-0.00000
27	O2	-0.00000	-1.00000	-0.00000
29	O2	0.00000	1.00000	-0.00000
30	O2	0.86603	0.50000	-0.00000
20	O2	-0.57735	1.00000	0.00000
21	O2	0.57735	1.00000	0.00000
23	O2	0.57735	-1.00000	0.00000
24	O2	-0.57735	-1.00000	0.00000
26	O2	-0.57735	1.00000	0.00000
27	O2	0.57735	1.00000	0.00000
29	O2	0.57735	-1.00000	0.00000
30	O2	-0.57735	-1.00000	0.00000
20	O2	0.00000	0.00000	1.00000
21	O2	-0.00000	-0.00000	-1.00000
23	O2	0.00000	0.00000	1.00000
24	O2	-0.00000	-0.00000	-1.00000
26	O2	0.00000	0.00000	1.00000
27	O2	-0.00000	-0.00000	-1.00000
29	O2	0.00000	0.00000	1.00000
30	O2	-0.00000	-0.00000	-1.00000
19	O2	1.00000	0.57735	0.00000
20	O2	0.50000	-0.28868	0.00000
21	O2	0.00000	0.57735	0.00000
22	O2	1.00000	-0.57735	0.00000
23	O2	-0.00000	-0.57735	0.00000
24	O2	0.50000	0.28868	0.00000
25	O2	1.00000	0.57735	0.00000
26	O2	0.50000	-0.28868	0.00000
27	O2	0.00000	0.57735	0.00000
28	O2	1.00000	-0.57735	0.00000
29	O2	-0.00000	-0.57735	0.00000
30	O2	0.50000	0.28868	0.00000
19	O2	1.00000	0.00000	0.00000
20	O2	0.25000	-0.43301	0.00000
21	O2	0.25000	0.43301	0.00000
22	O2	1.00000	0.00000	0.00000
23	O2	0.25000	-0.43301	0.00000
24	O2	0.25000	0.43301	0.00000
25	O2	1.00000	0.00000	0.00000
26	O2	0.25000	-0.43301	0.00000
27	O2	0.25000	0.43301	0.00000
28	O2	1.00000	0.00000	0.00000
29	O2	0.25000	-0.43301	0.00000
30	O2	0.25000	0.43301	0.00000
19	O2	0.00000	0.00000	1.00000
20	O2	-0.00000	-0.00000	-0.50000
21	O2	-0.00000	-0.00000	-0.50000
22	O2	-0.00000	-0.00000	-1.00000
23	O2	0.00000	0.00000	0.50000
24	O2	0.00000	0.00000	0.50000
25	O2	0.00000	0.00000	1.00000
26	O2	-0.00000	-0.00000	-0.50000
27	O2	-0.00000	-0.00000	-0.50000
28	O2	-0.00000	-0.00000	-1.00000

29	O2	0.00000	0.00000	0.50000
30	O2	0.00000	0.00000	0.50000

II. SUMMARY OF THE EXPERIMENTAL AND THEORETICAL PHONON FREQUENCIES AND DISPLACEMENT PATTERNS FOR $CO_4NB_2O_9$ AND THE TA ANALOG

Figure S1 summarizes the infrared response of $Co_4Nb_2O_9$ (a,c) and the Ta analog (b,d) as a function of temperature and polarization. The theoretically-predicted modes are on the top of each panel. Overall, we find very good agreement between the theoretical and experimental features, although a few modes overlap strongly making them hard to separate. Both $Co_4Nb_2O_9$ and $Co_4Ta_2O_9$ host the same space group, which explains the overall similarity in their phonon patterns. The primary difference is a mass effect due to having either Nb or Ta at the B site. As a result, the phonon modes involving these heavy elements will have slightly different frequencies. We also point out that the Ta analog displays a noisier spectrum which we attribute to the significantly smaller size of the single crystal. For completeness, we summarize the experimental and theoretical frequencies, mode symmetries, and mode displacement patterns below [Table S6]. There are no structural phase transitions within our sensitivity.

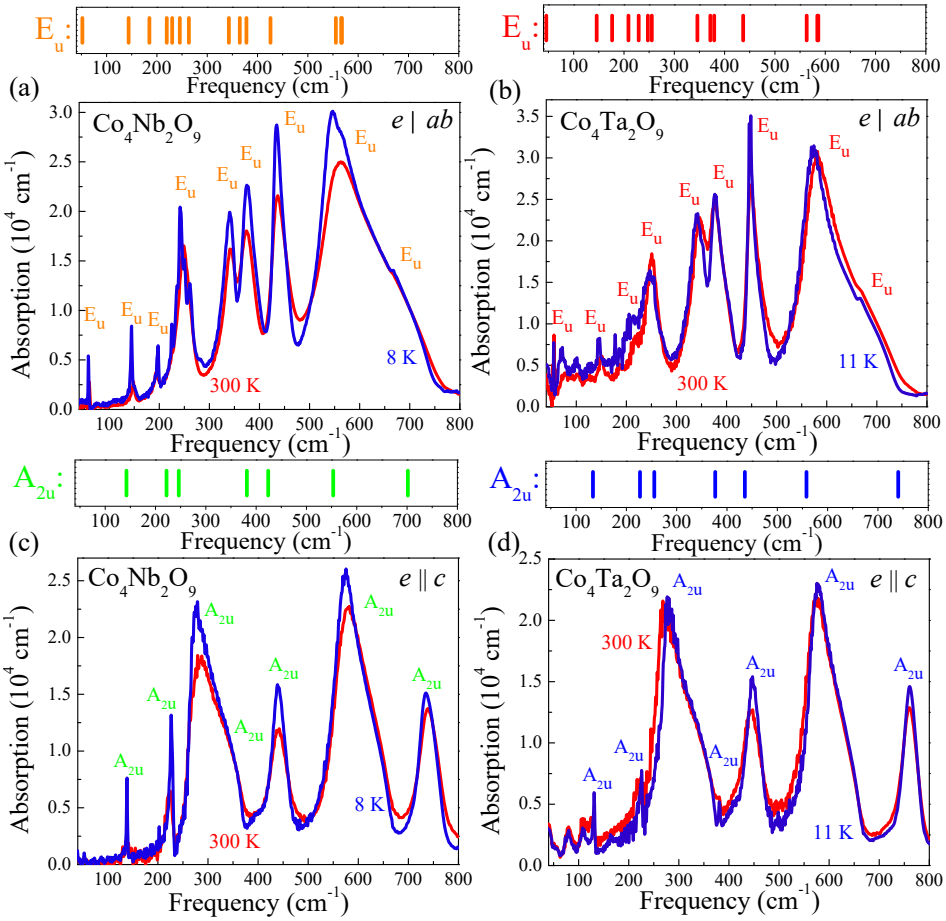

FIG. S1. Polarized infrared absorption spectra of $Co_4Nb_2O_9$ and $Co_4Ta_2O_9$. Red and blue curves represent high and low temperatures. (a,b) *ab*-plane polarized infrared spectra of $Co_4Nb_2O_9$ and the Ta analog. (c,d) *c*-axis polarized infrared spectra of $Co_4Nb_2O_9$ and the Ta analog. The calculated phonon frequencies for each compound and symmetry modes are on the top of every panel.

III. PHONONS AS A FUNCTION OF TEMPERATURE

Figure S2 displays a close-up view of precisely how the individual phonon modes of $Co_4Nb_2O_9$ change with temperature. In addition to using these trends to search for possible structural distortions, we employed the temperature dependence of these modes to track changes across the magnetic ordering transition. As discussed in the main text, only one phonon mode is sensitive to T_N. This is the E_u symmetry Co layer shearing mode near 150 cm^{-1} which

TABLE S6. Comparison of the experimental and theoretically predicted infrared-active phonon modes for $Co_4Nb_2O_9$. The same symmetries and displacement descriptions apply for $Co_4Ta_2O_9$.

Symmetry	Theoretical frequency (cm^{-1})	Experimental frequency (cm^{-1})	Mode displacement pattern
E_u	52	58	In-plane shearing of Co layer along B with a slight in-plane rocking of Nb_2O_3
A_{2u}	142	138	Out-of-plane Shearing of buckled Co layer against the rest of the lattice
E_u	144	145	In-plane shearing of Co planar and buckled layers
E_u	185	198	Twist of O-Co dimer
E_u	220	225	Internal shearing of Co buckled layer
A_{2u}	222	203	Shearing of planar Co againts the oxygen lattice
E_u	230	236	O-Nb-O bend
E_u	246	241	O-Co-O bend with twist
A_{2u}	246	226	Vertical motion of Co and N in sync, collective screw motion of O
E_u	264	250	Triangular breathing mode of two buckled Co and one Nb
E_u	343	261	O-Nb-O and O-Co-O bend
E_u	365	341	O-Nb-O bend
E_u	378	375	Oxygen layer shearing with a slight twist
A_{2u}	382	277	O-Nb-O bend in buckled Co layer
A_{2u}	424	440	In-phase O-Nb-O bend
E_u	426	434	In-plane motion of oxygen between buckled Co layers
E_u	553	546	In-phase oxygen motion in Co buckled layer against the rest of the lattice
A_{2u}	556	575	In-phase oxygen motion in buckled Co layer
E_u	566	566	Out-of-phase oxygen stretch
E_u	568	668	In-phase oxygen stretch
A_{2u}	702	735	Out-of-phase oxygen stretch

softens across the transition. This observation motivated our in-depth analysis of spin-phonon coupling. The other phonons display a normal anharmonic response as given by Eqn. 1 in the main text. All of the data are presented here for completeness. It is worth mentioning that there are important linewidth effects as well. An example is shown in Fig. S3. Here, narrowing linewidths with decreasing temperature give the appearance of splittings or local distortions when in fact, such detail is there all along (but unresolved). This can be shown by both oscillator strength and fitting analysis. We therefore conclude that the details in Fig. S3 derive from linewidth effects.

IV. SPIN-PHONON COUPLING IN $CO_4NB_2O_9$ AND THE TA ANALOG: SYMMETRY AND FRUSTRATION

For a detailed description of spin-phonon coupling in these systems, we can write out the various interactions using the diagram shown in Fig. S4. Using a pairwise analysis of the Co^{2+} centers, we can express the total spin-spin correlation function as a sum of the various ferromagnetic and antiferromagnetic interactions with individual λ's. Obviously, it is important to ascertain which terms are likely to be important and which interactions are less so.

We begin by emphasizing that there are two distinct layers (planar and buckled) in these materials. Further, we employ two different Co origins. With this framework and the diagram in Fig. S4, we can identify four unique coupling pathways. Here, we are ignoring interactions that are further away since these effects will likely be very small (essentially zero). For example, there is a long superexchange interaction along the c-axis between the Co^{2+} ions which we did not include because it is extremely weak. In any case, we see that a Co^{2+} origin in the planar layer yields three unique pathways. These include (i) the in-plane Co^{2+} ions that are edge-sharing, (ii) the out-of-plane Co^{2+} ions that are face-sharing, and (iii) the diagonal out-of-plane Co^{2+} ions that are corner-sharing. There is one more unique interaction (iv) that is within the buckled Co^{2+} layer. We assign the spin-phonon coupling constants for each of these interactions as $\lambda_{1,2,3,4}$ in as diagrammed in Fig. S4. Finally, we account for number of each type of interaction by multiplying $\lambda_{1,3,4}$ by three. This is the origin of the coefficients in the equations below. We can write down interactions as:

$$\lambda_{Total}\langle S_i \cdot S_j\rangle = 3\lambda_1\langle S_i \cdot S_j\rangle + \lambda_2\langle S_i \cdot S_j\rangle + 3\lambda_3\langle S_i \cdot S_j\rangle + 3\lambda_4\langle S_i \cdot S_j\rangle. \quad \text{(S1)}$$

In addition to identifying the four unique spin-phonon pathways, we can analyze the angle in each Co-O-Co linkage to assign the tendency for parallel or anti-parallel spin arrangement via the Goodenough-Kanamori-Anderson rules. We use the crystal structure of $Co_4Nb_2O_9$ as an example in order to assign ferromagnetic and antiferromagnetic

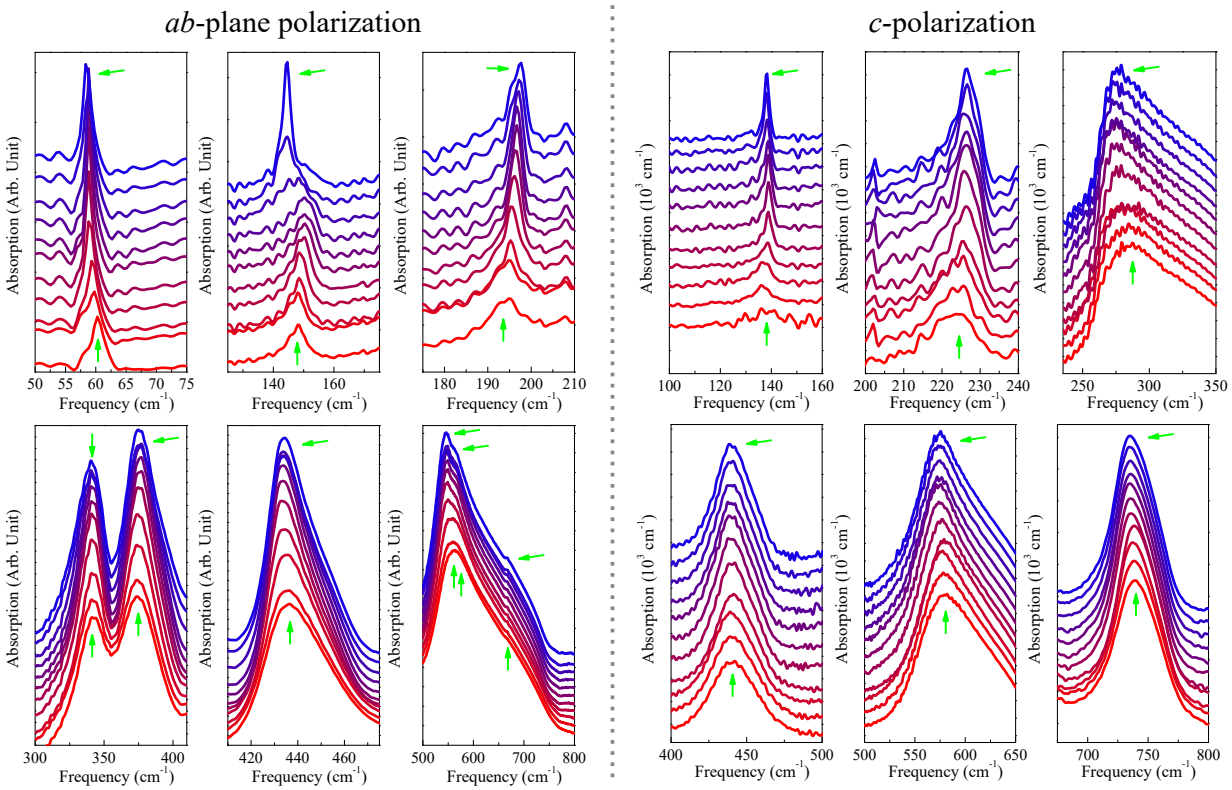

FIG. S2. Close-up views of the vibrational response of $Co_4Nb_2O_9$ as a function of temperature from 300 (red) to 4.2 K (blue). The green arrows point to where the phonon peak positions begin and end. Only the mode near 150 K softens across the magnetic ordering transition.

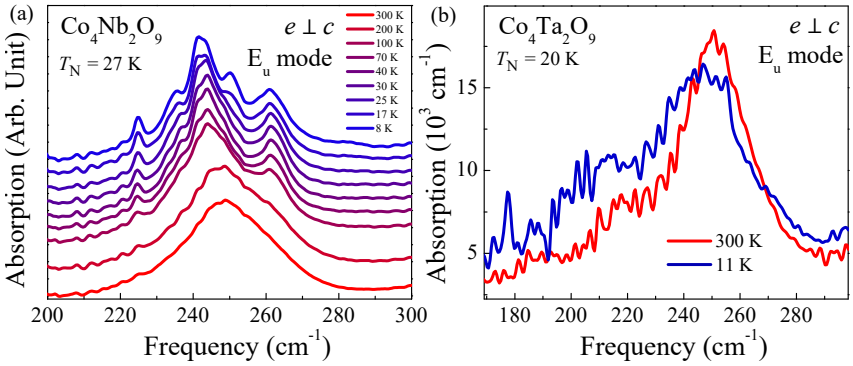

FIG. S3. (a) Stacked absorption spectra of $Co_4Nb_2O_9$. There are several phonon modes in the vicinity [Fig. 1, main text], and linewidth change give rise to the fine structure. (b) Absorption spectra of $Co_4Ta_2O_9$ at high and low temperatures. Unlike $Co_4Nb_2O_9$, the Ta analog does not have fine structure within our sensitivity - although the overall noise level is significantly higher.

tendencies. λ_1 and λ_2 have Co-O-Co angles of 90° and 83°, respectively. These are likely to be ferromagnetic superexchange interactions. λ_3 and λ_4 have Co-O-Co angles of 129° and 114°, respectively, with tendencies toward antiparallel alignment. In fact, it is well recognized that the antiferromagnetic interactions are the key to the overall magnetic structure in these compounds.[S3] In any case, we can now assign ferromagnetic (FM) or antiferromagnetic (AFM) interactions to the coupling constants as:

$$\lambda_{Total}\langle S_i \cdot S_j\rangle = 3\lambda_{1,FM}\langle S_i \cdot S_j\rangle + \lambda_{2,FM}\langle S_i \cdot S_j\rangle + 3\lambda_{3,AFM}\langle S_i \cdot S_j\rangle + 3\lambda_{4,AFM}\langle S_i \cdot S_j\rangle. \quad \text{(S2)}$$

The fact that this equation contains both ferromagnetic and antiferromagnetic terms indicates that the total spin-phonon coupling is likely to be frustrated. As a result, λ_{Total} will probably contain terms that both harden and soften the phonon across the magnetic ordering transition. The fact that we the 150 cm^{-1} mode softens across the magnetic ordering transition implies that antiferromagnetic interactions dominate.

We can simplify the expression in Eqn. SS2 by examining the phonon displacement pattern. As emphasized in the main text, the E_u symmetry vibrational mode near 150 cm^{-1} has a shearing motion. In other words, the Co^{2+} ions

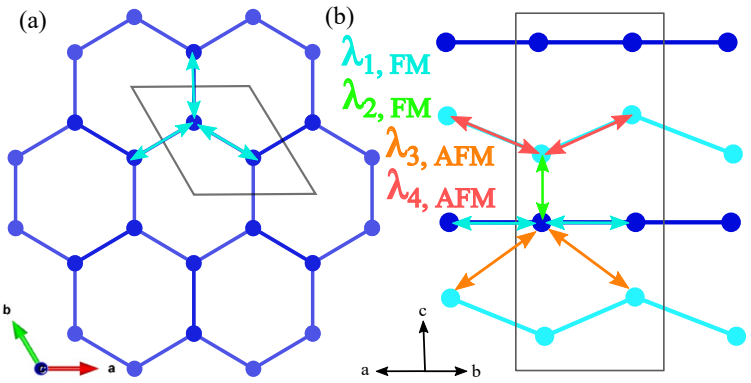

FIG. S4. (a) A simplified view of the planar Co^{2+} layer reveals a honeycomb-like structure and the in-plane near neighbor interactions. (b) This schematic illustrates both the planar and buckled layers. There are a total of two near-neighbor intralayer interactions and two near-neighbor interlayer interactions ($\lambda_{1,FM}$, $\lambda_{2,FM}$, $\lambda_{3,AFM}$, and $\lambda_{4,AFM}$). These interactions are shown in different colors. Note that we neglected the "long" interaction between Co centers along c because it is very weak.

in the planar layer move in one direction while those in the bucked layer move in the other. The key point is that although the planar and buckled layers oscillate in opposite directions [Fig. 2(e) in the main text], each layer moves together. The other important aspect is that the B site ions (Nb and Ta) are mostly fixed. The question then is exactly how the layer shearing mode modulates the Co centers. We find that symmetry plays a remarkable role in the breakdown of these interactions.

Let's begin by analyzing the simple back-and-form motion of the planar layer in isolation. All of the Co centers move together as part of this motion, but they do not move with respect to each other. As a result, the in-plane coupling constant $\lambda_{1,FM} = \partial^2 J_1/\partial u^2$ does not change with the motion. It is zero. We can apply the same argument to the buckled layer. The coupling constant in the buckled layer $\lambda_{4,AFM} = \partial^2 J_4/\partial u^2 = 0$. It too does not change with the motion of the 150 cm^{-1} phonon. It turns out that only the out-of-plane interactions are non-zero because coupling with the λ_2 and λ_3 terms survive.

Using these ideas, we can simplify the expression to read:

$$\lambda_{Total}\langle S_i \cdot S_j\rangle = \lambda_{2,FM}\langle S_i \cdot S_j\rangle + 3\lambda_{3,AFM}\langle S_i \cdot S_j\rangle. \tag{S3}$$

The key point is that this equation involves only inter-layer interactions as represented by λ_2 and λ_3. Furthermore, these λ have different tendencies. The competition between these ferromagnetic vs. antiferromagnetic contributions leads to magnetic frustration. Softening of the 150 cm^{-1} mode across the magnetic ordering transition is consistent with Goodenough-Kanamori-Anderson rules that relate orbital overlap to the exchange interaction J_{AFM} and a wider, more relaxed Co-O-Co bond angle.

V. PHONON LIFETIMES OF THE 150 CM^{-1} E_u SYMMETRY MODE AS A FUNCTION OF TEMPERATURE

In addition to frequency shifts which are discussed in great detail throughout this work due to their connection with spin-phonon coupling, the 150 cm^{-1} Co^{2+} layer shearing mode in both $Co_4Nb_2O_9$ and the Ta analog also hosts noticeable line width changes with decreasing temperature and across the magnetic ordering transition. The full width at half maximum of a phonon (Γ) is related to the phonon lifetime as:

$$\tau = \frac{\hbar}{\Gamma}. \tag{S4}$$

Here, τ is the phonon lifetime, Γ is the full width at half maximum, and $\hbar$ is the reduced Planck's constant.[S4] Focusing on the 150 cm^{-1} E_u symmetry shearing mode, the phonon lifetimes at room temperature are 0.75 and 0.6 ps for $Co_4Nb_2O_9$ and $Co_4Ta_2O_9$, respectively. This is shorter than what is usually found in traditional semiconductors and chalcogenides.[S5,S6] Typically, phonon lifetimes increase with decreasing temperature, but we observe the opposite trend in these materials [Fig. S5]. The phonon lifetime is determined by a combination of many different processes including three-phonon Umklapp, boundary, mass-difference, electron-phonon scattering, and spin-phonon scattering. By summing inverse lifetimes for each process, we can express $1/\tau$ as:

$$\frac{1}{\tau} = \frac{1}{\tau_u} + \frac{1}{\tau_b} + \frac{1}{\tau_m} + \frac{1}{\tau_{e-ph}} + \frac{1}{\tau_{s-ph}}, \tag{S5}$$

where τ_u is Umklapp, τ_b is boundary, τ_m is mass-difference, τ_{e-ph} is the electron phonon scattering, τ_{s-ph} is the spin-phonon scattering.[S5] We did not investigate individual contributions since this is beyond of the scope of our

work. That said, we note that the phonon lifetime exhibits a sudden increase below the Néel temperature, suggesting an important decrease in scattering events due to spin ordering.[S7]

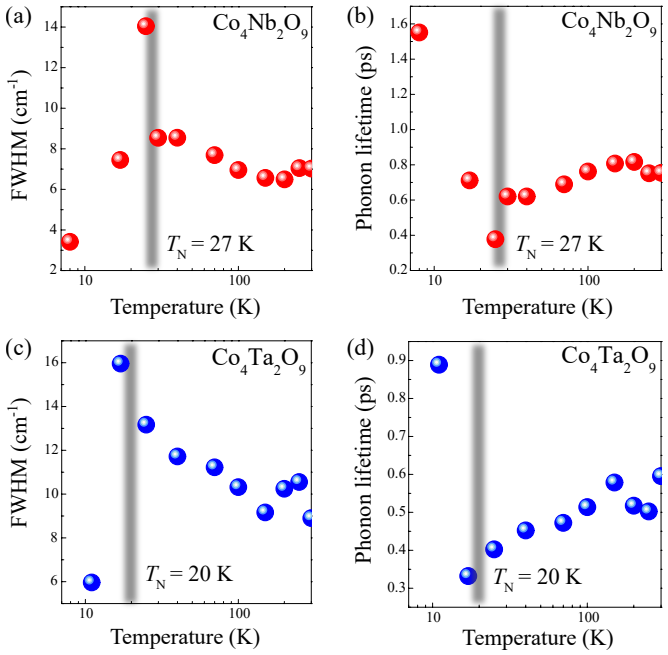

FIG. S5. Full width at half maximum (FWHM) and phonon lifetime for $Co_4Nb_2O_9$ (a, b) and the Ta analog (c, d) as a function of temperature. T_N is the magnetic ordering transition. Notice that temperature is shown on a log scale.

VI. SUPPLEMENTARY REFERENCES

[S1] E. Kroumova, M. Aroyo, J. Perez-Mato, A. Kirov, C. Capillas, S. Ivantchev, and H. Wondratschek, Phase Transitions **76**, 155 (2003).
[S2] H. T. Stokes, D. M. Hatch, and B. J. Campbell, SMODES, ISOTROPY Software Suite, iso.byu.edu.
[S3] I. V. Solovyev and T. V. Kolodiazhnyi, Phys. Rev. B **94**, 094427 (2016).
[S4] F. Wooten, *Optical Properties of Solids* (Elsevier, 1972).
[S5] Q. C. Sun, D. Mazumdar, L. Yadgarov, R. Rosentsveig, R. Tenne, and J. L. Musfeldt, Nano Letters **13**, 2803 (2013).
[S6] S. N. Neal, S. Li, T. Birol, and J. L. Musfeldt, npj 2D Materials and Applications **5**, 45 (2021).
[S7] A. Lunghi and S. Sanvito, Science Advances **5**, eaax7163 (2019).